Polymer Chemistry

ROYAL SOCIETY OF CHEMISTRY

PAPER

View Article Online
View Journal | View Issue

Cite this: *Polym. Chem.*, 2024, **15**, 5007

Reducing agent-triggered templated synthesis of a dynamic covalent poly(disulfide)s nanonetwork: remarkable tuning in noncovalent encapsulation stabilities and cargo release†

Arun Mondal, Sk Sujauddin, Dhiman Mondal, Soumya Kolay, Shuvajyoti Sarkar and Mijanur Rahaman Molla *

We demonstrated a new methodology for the templated synthesis of a crosslinked poly(disulfide)s-based dynamic covalent nanonetwork as a highly stable potential delivery vehicle for chemotherapeutic applications. The synthesis was carried out by treatment of a nanoaggregate of a biomass-derived lipoic acid-based amphiphilic monomer with a reducing agent at room temperature in open air and aqueous medium. The hydrodynamic diameter of the naoaggregate was ~130 nm as probed by dynamic light scattering. Control over the crosslinking density was achieved by varying the ratio of monomer : reducing agent. The crosslinking percentage varied from ~13% to ~100%. This provided the opportunity of fine-tuning the stability of the nanocarrier, noncovalent encapsulation stabilities and kinetics of cargo release, which are highly relevant in drug-delivery applications. For a highly crosslinked nanonetwork, in the simulated redox condition of cancer cells, ~80% release of the guest molecule was noted from the nanonetwork in a sustained manner. Controlled depolymerization of the polymer was accomplished by use of specific mol% of the same reducing agent. Finally, the reversibility and recyclability of the poly(disulfide)s to the monomeric form was achieved by treatment of the polymer with an external thiol in the presence of an organic base.

Received 4th October 2024,
Accepted 7th November 2024

DOI: 10.1039/d4py01109k

rsc.li/polymers

Introduction

The noncovalent encapsulation of a hydrophobic guest molecule in aqueous medium and its release in the desired location in response to a specific stimulus is the goal in drug-delivery applications.[1–6] For a robust delivery vehicle, the stability of the delivery vehicle itself and the encapsulation stability of the guest is critical in such a design.[7] Though polymeric micellar assemblies have been extensively studied for drug delivery, they have inherent stability issues. A micelle retains its structure only above a critical aggregation concentration (CAC). This phenomenon limits the practicality of *in vivo* use because high dilution is likely to occur while the nanocarrier is in the blood circulation, resulting in undesired release of the "payload" before reaching the target site.[8] Additionally, non-specific interactions of the micelle with the large protein molecules present in the blood can lead to disassembly followed by premature release of the guest.[9–11] The encapsulation stability of a polymeric micelle in aqueous medium is relatively poor.[12] To that end, a strategy of covalent crosslinking the core of a polymeric micelle[13–15] has been developed, but the degradability of the polymer backbone can be a limiting factor for its application.[12,16] Therefore, designing a completely degradable delivery vehicle with high stability even below the CAC, efficient encapsulation stability of the guest and controlled release are essential to avoid the complications of serious side effects in drug-delivery applications. However, some research teams (including our team) have shown that a combination of noncovalent supramolecular chemistry and dynamic covalent chemistry can lead to the formation of a completely degradable polymeric "nanonetwork". The latter stabilizes the small molecule-based nanoaggregate in a high dilution condition and minimizes the "leakiness" of the payload.[17–19] Here, we established a synthetic methodology for a series of crosslinked poly(disulfide)s termed "dynamic covalent nanonetwork" (NN). The poly(disulfide)s are known as "sustainable smart materials" due to the presence of multiple copies of dynamically reversible disulfide bonds. The disulfide bonds are readily cleavable and exchangeable in the presence of physical or chemical stimuli by overcoming the bond dissociation energy of 60 kcal mol^{-1}.[20] In the traditional synthesis of poly

Department of Chemistry, University of Calcutta, Kolkata-700009, India.
E-mail: mrmchem@caluniv.ac.in

† Electronic supplementary information (ESI) available. See DOI: https://doi.org/10.1039/d4py01109k

(disulfide)s, several stimuli, including heat, light, oxidizing agents, or thiol-based nucleophiles, are employed to induce polymerization.[21–26] In many cases, light is used exclusively to prepare a crosslinked network of poly(disulfide)s. Feringa and coworkers showed photo crosslinking of a 1,2-dithiolane ring and decrosslinking by a thiol.[27] The thiolate anion can effectively target and cleave disulfide bonds to promote the development of polymer chains through ring-opening polymerization (ROP). In 2011, Matile *et al.* pioneered the anionic ROP of 1,2-dithiolanes. They employed asparagusic acid (AA) units (a symmetric 1,2-dithiolane) as the terminal polymerizable moieties, which was polymerized by thiolate anions.[22] Liu and Moore *et al.* found that, in the presence of organic bases with substantial steric hindrance, alkyl thiolates created linear poly(1,2-dithiolane)s, while aryl thiolates produced cyclic species due to differences in the nucleophilicity of initiators.[23] Tian and Feringa *et al.* described the temperature-induced synthesis of a supramolecular polymer network of poly(disulfide)s from a thioctic acid monomer.[24] Yu and Liu *et al.* reported controlled and regioselective ROP of poly(disulfide)s by anion binding catalysis.[25] Lu and coworkers recently reported poly(disulfide)s synthesis in a frozen environment using a 1,2-dithiolane monomer and thiol from a protein to make a protein–poly(disulfide)s conjugate.[26]

Waymouth and coworkers reported thiol-initiated crosslinking of a micellar core formed by a 1,2-dithiolane ring.[28] Though there have been many reports of poly(disulfide)s, the control over the crosslinking density and "fine tuning" of the noncovalent encapsulation stabilities for crosslinked poly(disulfide)s of 1,2-dithiolane has not been explored. Here, we introduced a methodology for the synthesis of a series of core crosslinked poly(disulfide)s with variable crosslinking density by a reducing agent (dithiothreitol)-mediated ROP of the 1,2-dithiolane ring of lipoic acid (Scheme 1).[17–19] The use of a reducing agent generated a small percentage of thiol, which initiated the polymerization by ROP within the micelle core. Unlike light: (i) the crosslinking density could be controlled by varying the mol% of the reducing agent; (ii) crosslinking occurred at room temperature in open air and aqueous medium. This strategy enabled tunability in noncovalent encapsulation and guest release kinetics. Depolymerization was established by use of an excess of the same reducing agent. Finally, recyclability was achieved by regeneration of the monomer from the polymer in the presence of a thiol and organic base at room temperature.

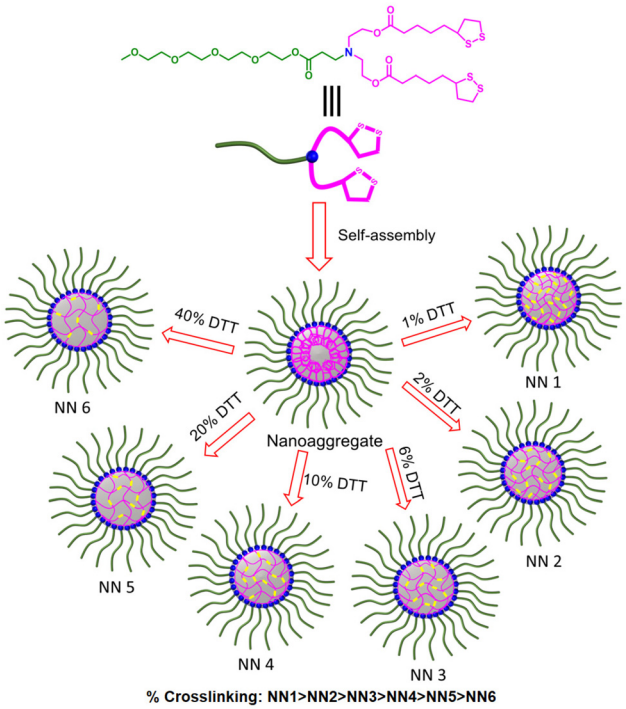

Scheme 1 Chemical structure of the lipoic acid-based amphiphile. Self-assembly in aqueous medium and fabrication of a crosslinked poly(disulfide)s nanonetwork by varying the mol % of dithiothreitol (DTT) (schematic).

Results and discussion

Aqueous self-assembly of the amphiphile

The nanoaggregate of the lipoic acid-based amphiphile (LPA) was prepared by self-assembly in water. In the nanoprecipitation technique, dropwise addition of water to an acetone solution of the amphiphile, followed by evaporation of acetone under stirring at room temperature, led to the formation of a self-assembled nanoaggregate of average hydrodynamic diameter of 130 nm as probed by DLS measurement (Fig. 1a). The range of average particle size obtained in the transmission electron microscopy (TEM) image was 100–120 nm (Fig. 1b), which agreed closely with the DLS data. A slightly smaller size

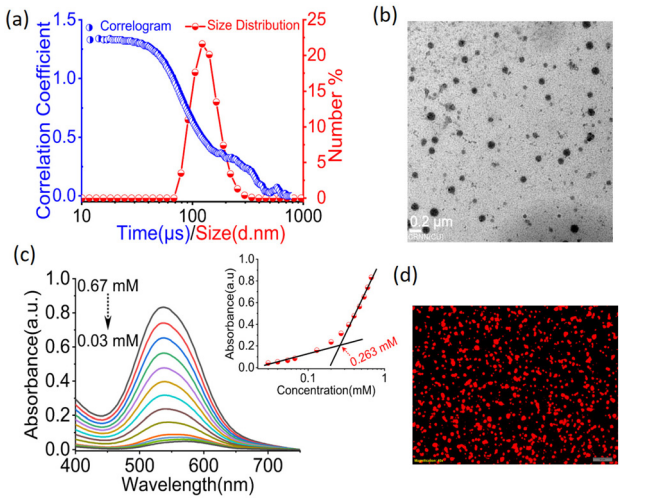

Fig. 1 (a) DLS profile of the self-assembled amphiphile (nanoaggregate). (b) TEM image of the nanoaggregate. (c) Nile-red absorption spectra by varying the concentration of LPA. Inset shows a plot of absorption intensity *vs.* concentration for CAC calculation (CAC = 263 μM). (d) Fluorescence microscopy image of a Nile red-encapsulated nanoaggregate.

in TEM data could be attributed to the shrinkage of the nanoparticle in the dried state.[29] Next, to probe the capability of guest encapsulation of this nanoaggregate, a hydrophobic model guest molecule, Nile red, was added to the solution of the nanoaggregate and the encapsulation was tested by the UV/visible spectroscopy. Nile red is not soluble in water unless a "hydrophobic shelter" is provided. However, Fig. 1c shows an intense absorption band of Nile red in water in the presence of the amphiphile solution, thus confirming formation of nanocontainer, which provided a hydrophobic shelter to Nile red. At a very low concentration of the amphiphile, an absorption band of Nile red was not observed but, after a certain concentration, 263 μM (*i.e.*, the CAC) (Fig. 1c, inset), a prominent band appeared and gradually became intense with an increasing concentration of the amphiphile. This phenomenon could be attributed to the encapsulation of more Nile-red molecules as a result of formation of a nanoaggregate beyond the CAC. The visual evidence of the Nile-red encapsulation was probed by fluorescence microscopy images, as shown by red particles in Fig. 1d.

Thermodynamics of self-assembly

We used an independent method of isothermal titration calorimetry (ITC) dilution to produce a thorough thermodynamic profile. We did this to obtain deeper understanding of nanoaggregate production *via* supramolecular assembly in water. This provides an opportunity of direct determination of thermodynamic parameters such as enthalpy, entropy and free energy of association. ITC is used extensively for the study of host–guest interactions,[30] but establishing the self-assembly use of ITC is quite recent.[31,32] The heat of change associated with the disassembly of the nanoaggregate (Fig. 2a) was determined in the ITC experiment. From the data, the enthalpy of aggregation and associated thermodynamic parameters were calculated using the equation mentioned in the experimental section.[34] The dilution experiment showed exothermic heat flow, which eventually was almost saturated beyond a specific concentration of the amphiphile designated as the CAC (288 μM) because disassembly of the micellar aggregates ceased (Fig. 2b). The CAC agreed well with the value obtained in the guest-encapsulation technique by UV/visible spectroscopy. The enthalpy change of demicellization calculated by the ITC experiment was −0.21 kcal mol^{-1} (Fig. 2c). Therefore, the negative enthalpy change indicated that the disassembly was an enthalpically favourable exothermic process and the self-assembly became an enthalpically unfavourable endothermic process. The entropy was calculated to be positive (15.50 cal mol^{-1} K^{-1}), so self-assembly was an entropically favourable process (Fig. 2d). The associated free energy was found to be negative (ΔG = −4.83 kcal mol^{-1}), thereby making the overall self-assembly a spontaneous process. The entropy-driven self-assembly could be attributed to the release of ester-bound water molecules into the bulk during self-assembly because the hydrophobic core of the self-assembled nanocontainer does not allow the polar water molecule to reside within the core.[33,34]

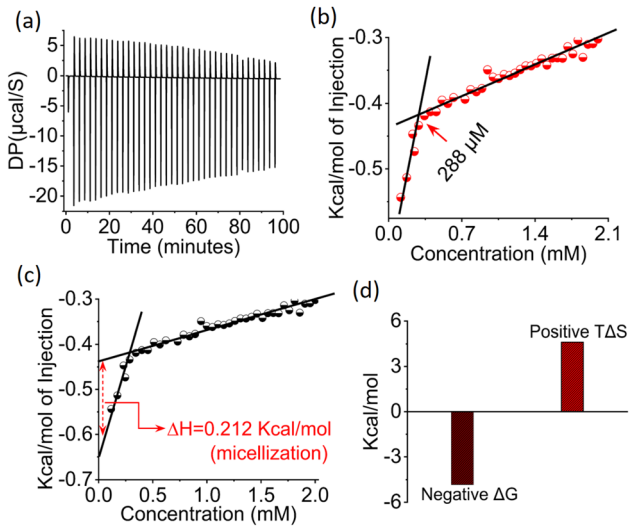

Fig. 2 (a) Measurement of heat release by ITC upon injection of a nanoaggregate solution of LPA into pure water at 298 K. (b) CAC determination from a plot of enthalpy *vs*. concentration. (c) Calculation of ΔH of aggregation from a plot of ΔH *vs*. concentration. (d) Plot showing negative ΔG and positive ΔS. Experimental temperature = 298 K.

Fabrication of a crosslinked poly(disulfide)s nanonetwork (NN), reducing agent-mediated depolymerization, external thiolate-induced recyclability and monomer recovery

Next, to construct a stable and dilution-insensitive nanoaggregate, we proposed to crosslink the core of the nanoaggregate consisting of 1,2-dithiolane rings by ROP. This strategy generated a dynamic covalent crosslinked poly(disulfide)s (*i.e.*, nanonetwork). In a typical experiment, first the aqueous solution of the nanoaggregate was treated with a calculated amount (1 mol%) of reducing agent, dithiotheitol (DTT), and stirred for 6 h at room temperature in open air. Crosslinking was monitored by UV/visible spectroscopy and size-exclusion chromatography. The disulfide in the 1,2 dithiolane ring and opened disulfide bond had distinct characteristic peaks at 335 nm and 280 nm, respectively. Hence, the 335 nm band corresponding to the cyclic monomer was monitored after the addition of DTT.[35] The band intensity at 335 nm gradually decreased with the progress of polymerization, as shown by the appearance of a new shoulder band at 280 nm upon addition of DTT (see the time-dependent UV/visible spectroscopy data in Fig. 3a). After 5 h of reaction, the spectra reached the saturation point, which indicated consumption of all the 1,2-dithiolane monomers. Here, at 1 mol% DTT, we assumed 100% crosslinking (see ESI† for detailed calculation of crosslinking percentage). The molecular weight (M_n) of this crosslinked polymer was calculated to be 259 000 g mol^{-1} by gel-permeable chromatography (GPC) and the nanonetwork was designated "NN1" (Fig. 3b). NN1 showed a spherical morphology with diameter in the range 100–120 nm as seen in the TEM image (Fig. 3c). However, use of >1 mol% DTT led to slow and controlled depolymerization, as seen by shifting of the dis-

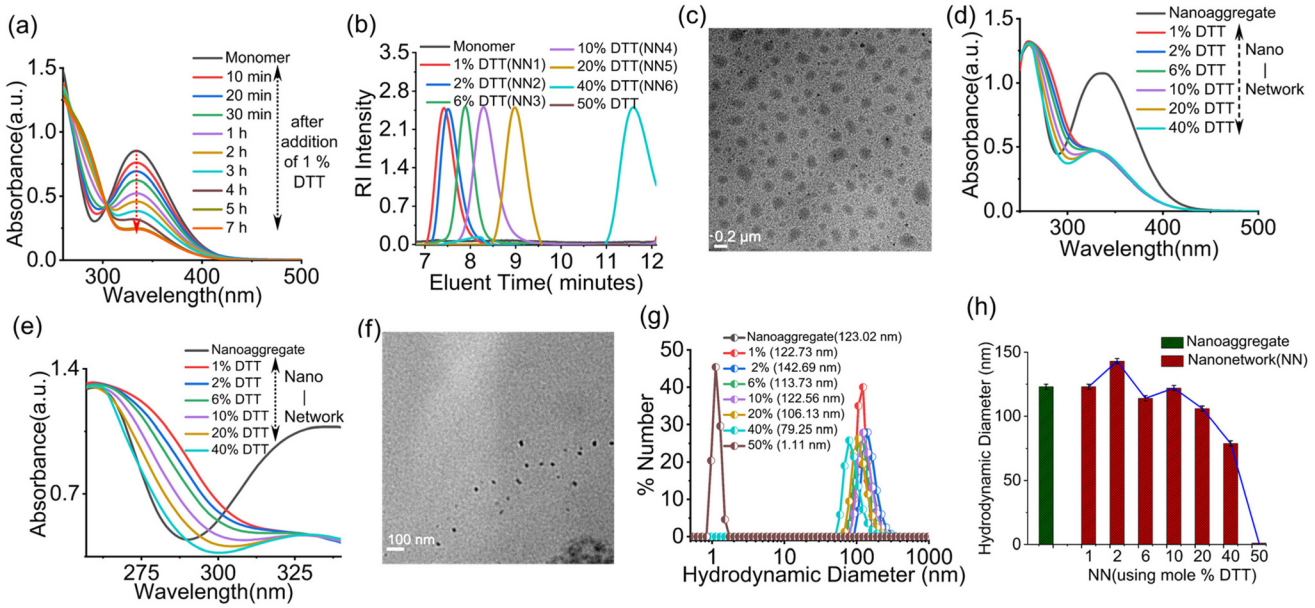

Fig. 3 (a) Polymerization kinetics by monitoring the absorption peak of the monomer at 335 nm using time dependent UV/visible spectroscopy upon addition of 1 mol% DTT in an aqueous solution of the LPA monomer. (b) GPC profile of crosslinked poly(disulfide)s by varying the mol% of DTT. (c) TEM image of a poly(disulfide)s nanonetwork (1 mol% DTT). (d) Plot of absorption spectra of all poly(disulfide)s nanonetworks and (e) zoomed version of the plot in (d), indicating a decrease in polymer-band intensity with increasing mol% of DTT. (f) Complete depolymerization at 50 mol% DTT shown by the corresponding TEM image, which revealed no aggregate structure. (g) Comparison of the DLS profile of the nanoaggregate, all nanonetworks and the depolymerized solution. (h) Bar-chart representation of the DLS profile presented in (g).

tribution curve in the SEC chromatogram towards lower molecular weight (Fig. 3b). Here, the reduction of the absorption intensity corresponding to the open-chain disulfide bonds at 280 nm further confirmed slow depolymerization and formation of free thiol (Fig. 3d and e). For the nanonetwork fabrication, a variable amount of DTT was used (1, 2, 6, 10, 20 or 40 mol%) and corresponding nanonetwork was assigned as "NN1", "NN2", "NN3", "NN4", "NN5" and "NN6", respectively (Fig. S1†). Until 10 mol% DTT (NN4), the nanonetwork could uphold 50% crosslinking (~86% and 74% for NN2 and NN3, respectively) but, for NN4 and NN6, the crosslinking dropped to 32% and 13%, respectively (see ESI† for detailed calculations). The visual evidence of encapsulation of Nile red for all crosslinked nanonetworks is given in Fig. S2.†

Further, 50 mol% DTT was used for complete depolymerization of the poly(disulfide)s network. From NN1 to NN6, the molecular weight gradually decreased from 259 000 to 3600 g mol^{-1} but, at 50 mol% DTT, the SEC band corresponding to the polymer disappeared and became a straight line, indicating complete depolymerization of the poly(disulfide)s network (Fig. 3b). Hence, beyond 1 mol% DTT, slow depolymerization decreased the crosslinking density, and complete depolymerization at 50 mol% DTT diminished the nanonetwork structure. This conclusion was further supported by the morphology according to TEM, whereby defined particle structure was not observed after treatment of a nanonetwork with 50 mol% DTT (Fig. 3f). The slow depolymerization with increasing mol% of reducing agent was also probed with the measurement of hydrodynamic diameter by DLS. This experiment revealed gradual decrease in the average hydrodynamic diameter of the nanonetwork from ~123 to ~1 nm (Fig. 3g and h). Therefore, the size of ~1 nm in the case of 50 mol% DTT suggested complete depolymerization. Fig. 4a shows that use of higher mol% of DTT led to faster consumption of the monomer due to increased contribution in the consumption by the DTT-mediated direct reduction of disulfide bonds in the 1,2-dithiolane ring. Particularly in the case of 40 mol% or 50 mol% DTT, Fig. 4b and

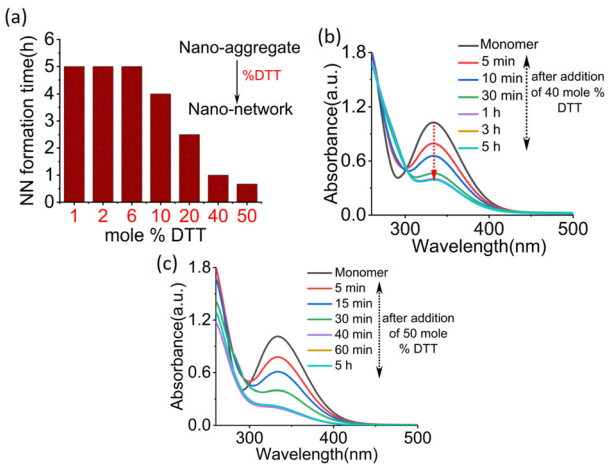

Fig. 4 (a) Time profile for nanoaggregate-to-nanonetwork conversion in the presence of various mol% of DTT. Time-dependent UV/visible spectra after treatment of the monomer with (b) 40 mol% and (c) 50 mol% DTT.

c no not show a shoulder band at 280 nm corresponding to open-chain disulfides in the polymer, instead a straight line is shown. This can be attributed to a reduction of most of the disulfide bonds in the polymer and formation of the free thiol. The presence of the free thiol indicates depolymerization and, in principle, the greater the amount of free thiol, the greater the depolymerization. According to UV/vis spectra, 100% crosslinking occurred in NN1, gradual decrosslinking occurred from NN2 to NN6, and total decrosslinking occurred at 50% DTT.

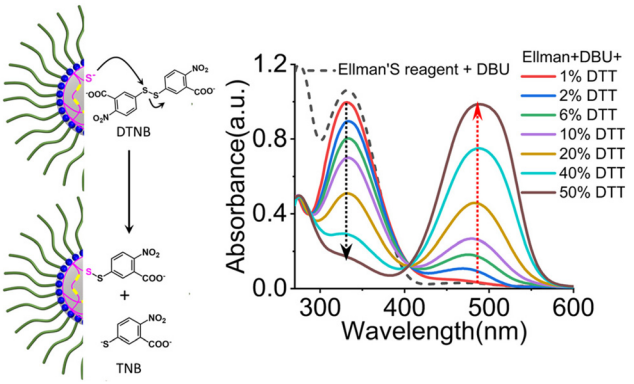

Fig. 5 Testing for the presence of free thiol after nanonetwork fabrication. In 1 mol% DTT, no peak of TNB indicates the absence of thiol (*i.e.*, maximum crosslinking) whereas, with an increasing mol% of DTT, free thiol content increases as indicated by increasing intensity of TNB (*i.e.*, little crosslinking). The chemical structure of the reaction of free thiol with Ellman's reagent is shown schematically on the left.

Therefore, we expected the absence of free thiol in NN1 and presence of maximum free thiol in the complete decrosslinked solution (50% DTT). To probe the thiol content in the solution, we carried out a very well-known Ellman's test (Fig. 5).[36] Upon addition of Ellman's reagent to the NN solution in the presence of a base, a significant band at 490 nm that corresponded to 2-nito-5-thiobenzoate (TNB) appeared, and the original Ellman's reagent or DTNB band vanished, suggesting the existence of free thiol as a result of depolymerization. It's interesting to note that in the case of NN1, a band corresponding to TNB was not seen, indicating the absence of free thiol in the NN1 solution. Even though the concentrations of Ellman's reagent in each solution were identical, the strength of the TNB band increased progressively from NN2 to NN6. This could be attributed to the increasing concentration of the free thiol due to higher percentage of decrosslinking in moving from NN2 to NN6. The maximum intensity of the TNB peak and almost complete disappearance of the DTNB peak at 50 mol% DTT suggested the highest percentage of depolymerization compared with other nanonetworks.

Upon addition of an external thiolate anion to the solution of the nanonetwork, the thiolate anion cleaved the disulfide bonds, which then closed to reform the 1,2-dithiolane ring containing the monomer (see the scheme in Fig. 6a), as indicated by evolution of the distinct peak at 335 nm in UV/visible spectroscopy (Fig. 6b). This indicates recovery of the monomer. The profile of size-exclusion chromatography showed disappearance of the bands corresponding to the polymer, thus further suggesting thiolate anion-induced depolymerization (Fig. 6c). To obtain direct proof for the formation of the monomer, we performed liquid chromatography-mass

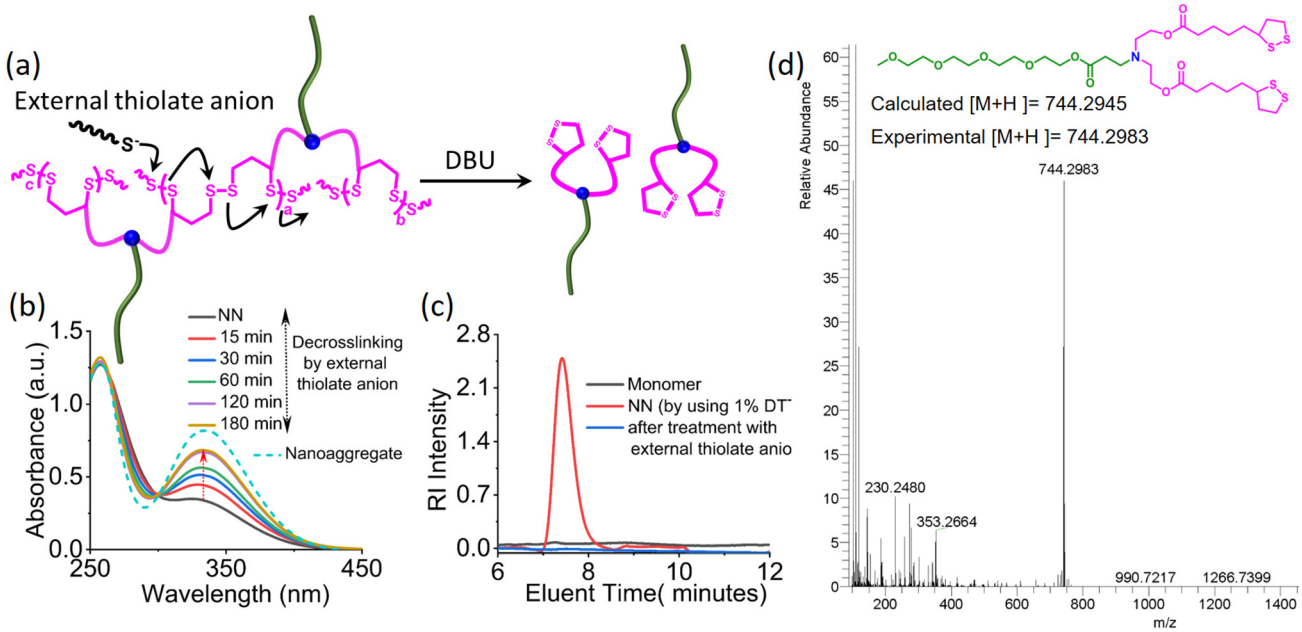

Fig. 6 (a) Depolymerization by an external thiol in the presence of a DBU base (schematic). (b) Monitoring depolymerization by UV/visible spectroscopy, which shows increasing band intensity corresponding to the monomer at 335 nm. (c) GPC profile of poly(disulfide)s and depolymerized solution. (d) LC-MS profile of the depolymerized solution. Solvent for the column for GPC = DMF; measurement temperature = 30 °C.

spectrometry (LC-MS), which revealed a distinct peak at 744.29 g mol^{-1} corresponding to the lipoic acid-based monomer (Fig. 6d), thus suggesting reversibility and reformation of the monomer.

Stability of the crosslinked poly(disulfide)s nanonetwork

Furthermore, we examined the stability of the nanonetwork itself and compared it with the nanoaggregate. We showed that the crosslinking had a tremendous effect on the stability of the nanocarrier. Here, we used the moderately crosslinked nanonetwork (NN2) for this study. To that end, the nanoaggregate and NN2 were diluted with water, and systematic changes in the size were monitored by DLS. Interestingly, the nanonetwork retained its structure even below the CAC, while nanoaggregates disassembled below the CAC and an aggregate structure was not observed in the DLS profile, thereby suggesting the very high stability and dilution insensitivity of the nanonetwork (Fig. 7a and Fig. S3†). To further validate the structural integrity of the nanonetwork in a good organic solvent such as dimethylformamide (DMF), the nanonetwork and nanoaggregate were diluted with DMF and the DLS profile was recorded. The nanonetwork persisted even below the CAC, but nanoaggregates were completely dissolved and no particle was detected by DLS (Fig. 7b and Fig. S4†). Here, a slight increase in the size of the nanonetwork could be attributed to the swelling of the crosslinked structure in an organic solvent. Hence, crosslinking the core of the nanoaggregate increased the stability towards dilution markedly.

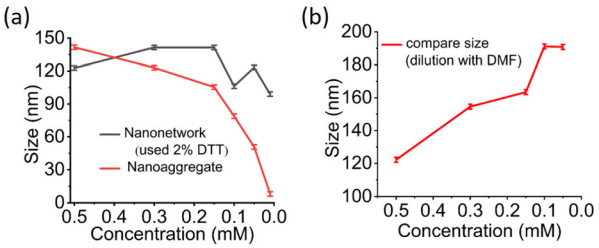

Fig. 7 (a) Probing the dilution tolerance of the nanoaggregate and nanonetwork in water by measuring the DLS profile with dilution. (b) Testing the stability of the nanonetwork by dilution with the organic solvent DMF. In both cases, the nanonetwork showed stability below the CAC.

Tunability in noncovalent encapsulation stability

To probe the tunability in guest encapsulation stabilities by controlling the crosslinking densities, the very well established fluorescence resonance energy transfer (FRET) was carried out using a lipophilic FRET pair: 3,3′-dioctadecyloxacarbocyanine per chlorate (DiO, donor) and 1,1′-dioctadecyl-3,3,3′,3′-tetramethylin docarbocyanine perchlorate (DiI, acceptor) (see Fig. 8a for the scheme).[37,38] In a typical FRET experiment, DiO and DiI were co-encapsulated in the core of the nanoaggregate and, by varying the amount of DTT, FRET pair-loaded nanonetworks were prepared. Upon excitation of the donor molecule (DiI) at 450 nm, strong emission of the acceptor at 580 nm was noticed due to the energy transfer from the donor to the acceptor because they were within the Froster distance within the nanonetwork (Fig. 8b, c and Fig. S5†). Time-dependent FRET was recorded and, to obtain information about the encapsula-

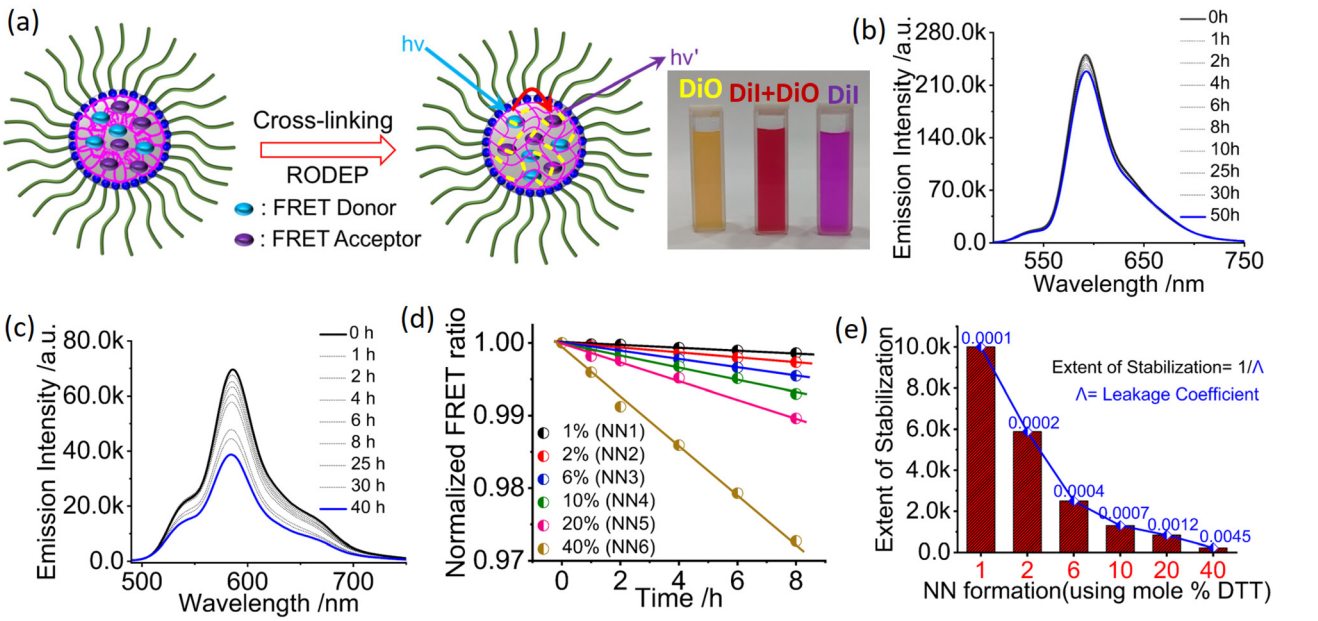

Fig. 8 (a) FRET by co-encapsulating DiI and DiO within the nanonetwork core (schematic). Images of the nanonetwork solution individually and loaded with a mixture of DiI and DiO. Monitoring of FRET by emission spectroscopy for the nanonetwork formed by (b) 1 mol% and (c) 40 mol% of DTT. (d) Calculation and comparison of the leakage coefficient of all nanonetworks from normalized FRET ratio *vs.* time plot. (e) Plot of leakage coefficient *vs.* various nanonetworks (NN1 to NN6).

tion stability, the leakage coefficient was calculated from the slope of the plot of normalized FRET ratio *vs.* time (Fig. 8d). A very low leakage coefficient for the 100% crosslinked nanonetwork (NN1) was observed, whereas nanonetwork with the lowest crosslinking density (NN6) showed a high leakage coefficient (*i.e.*, low encapsulation stability) (Fig. 8e).[39,40] Furthermore, we hypothesized that the guest encapsulation efficiency (EE) and encapsulation capacity (EC) would be highly dependent on the crosslinking density. To test this hypothesis, we measured the EE and EC for all nanonetworks and interestingly found that EE and EC gradually increases from NN6 to NN1 (Fig. S6†). This can be attributed to the increasing crosslinking density from NN6 to NN1.

Tunability in stimuli-responsive guest release

To check stimuli-responsive guest release, it is imperative to obtain detailed information regarding the degradation profile of the nanocarrier. After careful evaluation of the guest encapsulation stability, we examined the redox-responsive degradation of the poly(disulfide)s nanonetwork by DLS and SEC (Fig. 9a, b and Fig. S7†). Notably, treatment of the nanonetwork with a simulated concentration (10 mM) of glutathione found in cancer cells[41] resulted in the disappearance of the band in SEC, transforming it into a straight line, which signified the degradation of crosslinked disulfide bonds and disintegration of the polymeric structure. Treatment of the nanonetwork with GSH (10 mM) and analysis of time-dependent DLS indicated a reduction in hydrodynamic size from ~142 nm to ~5 nm, implying disintegration of the poly(disulfide) network and generation of tiny molecular fragments. In a control experiment, application of a modest quantity of GSH (10 μM), pertinent to blood serum, did not alter the SEC profile or hydrodynamic size, thereby showing a selective reaction and destruction of the nanonetwork in a cancer-relevant redox environment.

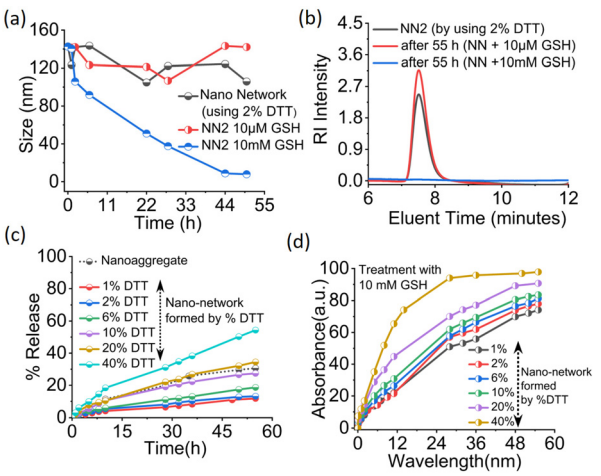

Fig. 9 (a) Stability and degradation of nanonetworks under different GSH concentrations measured by DLS. (b) GPC profile of nanonetworks after and before treatment with various concentrations of GSH. Percent release of guest for all the nanonetwork and nanoaggregates in the (c) absence of GSH and (d) presence of GSH.

Upon comprehending the redox-responsive degradation mechanism, we investigated the potential for regulated release of the guest through decrosslinking followed by disassembly in the presence of GSH. The hydrophobic dye Nile red was utilized as a "model" guest molecule, and guest release was tracked using UV/visible spectroscopy because Nile red has a unique band at 550 nm that decreases with time after treating the nanonetwork with GSH. This effect could be attributed to precipitation of Nile red as soon as it exits the hydrophobic shelter of the nanonetwork. The computation for guest-release percentage indicated almost 72% release for the NN1 nanocarrier during the course of 55 h. However, the rate of release increased progressively from NN1 to NN6, with a notable rise noted for NN5 and NN6 (Fig. 9c and Fig. S8†). Leakiness was correlated with an increasing release rate, and lower crosslinking densities caused higher leakiness for NN5 and NN6. On the other hand, in the absence of GSH, ~55% release was observed for NN6, while NN1 showed only ~12% release of the guest molecule. This high stability of NN1 in the dormant state could be attributed to the high crosslinking density (Fig. 9d and Fig. S9†). For the nanoaggregate, the value was found to be 32%, which again indicated that crosslinking increased the noncovalent encapsulation stability. Therefore, the concept of direct proportionality of noncovalent encapsulation stability with the crosslinking density was established by the above-discussed experiments.

Conclusions

We developed a methodology for the templated synthesis of crosslinked poly(dislulfide)s by reducing agent (DTT)-induced ROP of the 1,2-dithiolane ring present at the core of a micelle of a biomass-derived lipoic acid-based amphiphilic monomer at room temperature in aqueous medium and open air. The advantages of this method were: (i) polymerization in open air, room temperature and aqueous medium; (ii) fine tuning of crosslinking density by maintaining the ratio of monomer : reducing agent. Complete depolymerization was achieved by use of a specific amount of the same reducing agent, which was established by UV/visible spectroscopy, DLS, TEM and SEC. The nanonetwork showed no effect on the dilution even below the CAC of the corresponding self-assembled structure. It also retained its nanostructure morphology upon dilution by good organic solvent such as DMF. Therefore, in terms of the stability of the nanocarrier, the combination of noncovalent interactions and covalent chemistry to form the nanonetwork was advantageous over the nanoassemblies formed by only noncovalent interactions. Here, a series of poly(disulfide)s-based nanonetworks (NN1 to NN6) obtained by varying the crosslinking percentage were fabricated. We studied their stability and noncovalent encapsulation stability. The higher the percentage of crosslinking, the higher was the noncovalent encapsulation stability according to FRET experiments and calculation of the leakage coefficient. The encapsulation efficiency and encapsulation capacity followed similar trends. Hence, by varying the crosslinking density of the nanonetwork,

the stability of the noncovalent encapsulation could be tuned and the GSH-mediated release kinetics of the guest molecules could be controlled. The detailed biological application of this nanonetwork towards targeted drug delivery to cancer cells is underway in our research team. We believe that dynamic formation of a covalent poly(disulfide)s-based nanonetwork with high stability (even below the critical micellar concentration), high noncovalent encapsulation stability and tunable release kinetics will aid design of a robust delivery vehicle for chemotherapeutic applications.

Author contributions

Arun Mondal: synthesis, characterization, physical-chemistry experiments, data collection/analysis, and preparation of the draft manuscript. Sk. Sujauddin, Dhiman Mondal and Shuvajyoti Sarkar: supported some physical-chemistry experiments. Soumya Kolay: supported TEM experiments. Mijanur Rahaman Molla: conceptualization, acquisition of funds, supervision of whole work, review/finalization of the manuscript.

Data availability

The data supporting the conclusions reached in this study have been included as part of the ESI.†

Conflicts of interest

There are no conflicts of interest to declare.

Acknowledgements

AM thanks CSIR-India for his fellowship. SKS and SS thank the UGC for their fellowships. MRM thanks the DST-SERB for funding (TAR/2022/000020). The authors thank Professor Dilip Kumar Maiti (University of Calcutta) for helping with DLS facilities. The instrumental and infrastructural facilities were provided by the University of Calcutta, India.

References

1 M. A. Beach, U. Nayanathara, Y. Gao, C. Zhang, Y. Xiong, Y. Wang and G. K. Such, *Chem. Rev.*, 2024, **124**, 5505–5616.
2 D. Peer, J. M. Karp, S. O. C. Hong, R. F. Margalit and R. Langer, *Nat. Nanotechnol.*, 2007, **2**, 751–760.
3 S. Mura, J. Nicolas and P. Couvreur, *Nat. Mater.*, 2013, **12**, 991–1003.
4 T. M. Allen and P. R. Cullis, *Science*, 2004, **303**, 1818–1822.
5 S. Santra, S. Das, S. Dey, A. Sengupta, B. Giri and M. R. Molla, *Biomacromolecules*, 2024, **25**, 1724–1737.
6 M. R. Molla, P. Rangadurai, G. M. Pavan and S. Thayumanavan, *Nanoscale*, 2015, **7**, 3817–3837.
7 R. Savic, A. Eisenberg and D. J. Maysinger, *J. Drug Targeting*, 2006, **14**, 343–355.
8 Y. H. Bae and H. J. Yin, *Controlled Release*, 2008, **131**, 2–4.
9 H. Chen, S. Kim, L. Li, S. Wang, K. Park and J. X. Cheng, *Proc. Natl. Acad. Sci. U. S. A.*, 2008, **105**, 6596–6601.
10 H. Chen, S. Kim, W. He, H. Wang, P. S. Low, K. Park and J. X. Cheng, *Langmuir*, 2008, **24**, 5213–5217.
11 P. Xu, E. Gullotti, L. Tong, C. B. Highley, D. R. Errabelli, T. Haasan, J. X. Cheng, D. S. Kohane and Y. Yeo, *Mol. Pharmaceutics*, 2009, **6**, 190–201.
12 S. Jiwpanich, J. H. Ryu, S. Bickerton and S. Thayumanavan, *J. Am. Chem. Soc.*, 2010, **132**, 10683–10685.
13 L. Wu, Y. Zou, C. Deng, R. Cheng, F. Meng and Z. Zhong, *Biomaterials*, 2013, **34**, 5262–5272.
14 F. Calik, A. Degirmenci, M. Eceoglu, A. Sanyal and R. Sanyal, *Bioconjugate Chem.*, 2019, **30**, 1087–1097.
15 Y. Olszowy, J. Wesselmann, S. F. Over, F. Pätzold and R. Weberskirch, *Polym. Chem.*, 2023, **14**, 3761–3774.
16 Y. Liu, M. Chen, G. Li, S. Xu and H. Liu, *Langmuir*, 2023, **39**, 12671–12679.
17 A. Mondal, S. Das, S. M. Ali, S. Kolay, A. Sengupta and M. R. Molla, *Bioconjugate Chem.*, 2023, **34**, 489–500.
18 C. Liao, Y. Chen, Y. Yao, S. Zhang, Z. Gu and X. Yu, *Chem. Mater.*, 2016, **28**, 7757–7764.
19 J. Huang, F. Wu, Y. Yu, H. Huang, S. Zhang and J. You, *Org. Biomol. Chem.*, 2017, **15**, 4798–4802.
20 G. Gaydon, *Dissociation Energies and Spectra of Diatomic Molecules*, Chapman and Hall, London, 2nd edn, 1953.
21 J. Cao and D. C. Chen, *Phys. Chem. Chem. Phys.*, 2019, **21**, 4176.
22 N. Sakai, M. Lista, O. Kel, S. I. Sakurai, D. Emery, J. Mareda, E. Vauthey and S. Matile, *J. Am. Chem. Soc.*, 2011, **133**, 15224–15227.
23 Y. Liu, Y. Jia, Q. Wu and J. S. Moore, *J. Am. Chem. Soc.*, 2019, **141**, 17075–17080.
24 Q. Zhang, C. Y. Shi, D. H. Qu, Y. T. Long, B. L. Feringa and H. Tian, *Sci. Adv.*, 2018, **4**, aat8192.
25 T. Du, B. Shen, J. Dai, M. Zhang, X. Chen, P. Yu and Y. Liu, *J. Am. Chem. Soc.*, 2023, **145**, 27788–27799.
26 J. Lu, H. Wang, Z. Tian, Y. Hou and H. Lu, *J. Am. Chem. Soc.*, 2020, **142**, 1217–1221.
27 B. Sieredzinska, Q. Zhang, K. J. van den Berg, J. Flapper and B. L. Feringa, *Chem. Commun.*, 2021, **57**, 9838–9841.
28 X. Zhang and R. M. Waymouth, *J. Am. Chem. Soc.*, 2017, **139**, 3822–3833.
29 A. O. Moughton and R. K. O'Reilly, *Chem. Commun.*, 2010, **46**, 1091–1093.
30 C. Qian, S. Zhang, J. Li, B. Zuo and X. Wang, *Soft Matter*, 2014, **10**, 1579–1590.
31 D. Görl and F. Würthner, *Angew. Chem., Int. Ed.*, 2016, **55**, 12094–12098.
32 P. P. N. Syamala, B. Soberats, D. Görl, S. Gekle and F. Würthner, *Chem. Sci.*, 2019, **10**, 9358–9366.
33 P. Dey, P. Rajdev, P. Pramanik and S. Ghosh, *Macromolecules*, 2018, **51**, 5182–5190.

34 S. Santra, A. Ghosh, A. Mondal, S. M. Ali, D. Das, K. Sarkar, L. Roy and M. R. Molla, *ACS Appl. Polym. Mater.*, 2022, **4**, 7614–7625.
35 S. Maes, V. Scholiers and E. F. DuPrez, *Macromol. Chem. Phys.*, 2023, **224**, 2100445.
36 J. Lu, S. C. Owen and M. S. Shoichet, *Macromolecules*, 2011, **44**(15), 6002–6008.
37 S. Kolay, M. Das, A. Mondal, A. Sengupta, A. S. Bag, P. De and M. R. Molla, *Biomacromolecules*, 2024, **25**, 5068–5080.
38 K. Dan, P. Rajdev, J. Deb, S. S. Jana and S. Ghosh, *J. Polym. Sci., Part A: Polym. Chem.*, 2013, **51**, 4932–4943.
39 P. Kuppusamy, H. Q. Li, G. Ilangovan, A. J. Cardounel, J. L. Zweier, K. Yamada, M. C. Krishna and J. B. Mitchell, *Cancer Res.*, 2002, **62**, 307–312.
40 A. N. Koo, K. H. Min, H. J. Lee, S. U. Lee, K. Kim, I. C. Kwon, S. H. Cho, S. Y. Jeong and S. C. Lee, *Biomaterials*, 2012, **33**, 1489–1499.
41 R. Mo and Z. Gu, *Mater. Today*, 2016, **19**, 274–283.